Preprint

A quasi-decadal pulse linking geomagnetic pole drift and global temperature: HAC-robust multivariate evidence and break diagnostics (1981–2024)

Authors:
Antonio Iadicicco

Version of record (Zenodo DOI):	https://doi.org/10.5281/zenodo.18688127
SpinScience ID:	spinscience:2026.000002
Version:	v1
Year:	2026
License:	CC BY 4.0
Record:	—

A quasi-decadal pulse linking geomagnetic pole drift and global temperature: HAC-robust multivariate evidence and break diagnostics (1981–2024)

Antonio Iadicicco[1], *et al.*
[1]Università Popolare Nikola Tesla (UniTesla), Italy

Highlights

- A reproducible statistical "pulse" emerges between geomagnetic pole-speed proxies and GMST once dominant controls are included (1981–2024, $n = 44$).
- A HAC-robust multivariate model explains $\approx 92\%$ of GMST variance ($R^2 = 0.923$, adj. $R^2 = 0.912$).
- The dipole pole-speed coefficient is negative and remains significant under alternative geomagnetic-activity controls (aa vs ap; HAC $p \approx 0.03$).
- Break scans flag distinct candidate change-years in GMST (2008) and pole-speed proxies (1996/2006), consistent with time-varying coupling.
- In the 8–13y band, a low-degree "core proxy" (IGRF $n \leq 3$ PC1) aligns with pole-speed ($r \approx 0.78$) and also with GMST ($r \approx 0.61$), motivating mechanistic follow-up.

Abstract

Do the planet's magnetic choreography and surface-temperature variability share a faint common rhythm? We test for reproducible co-variation between annual global-mean surface temperature (GMST) and geomagnetic dynamics using geomagnetic pole-speed proxies derived from IGRF-13, together with standard physical controls (CO_2 radiative forcing, ENSO, cosmic-ray neutrons, geomagnetic activity indices). On the 1981–2024 annual sample ($n = 44$), a multivariate OLS model with Newey–West HAC covariance (maxlags=3) achieves $R^2 = 0.9225$ (adj. $R^2 = 0.9123$). The standardized coefficient for dipole pole-speed is negative and remains statistically significant when replacing aa with ap as the geomagnetic-activity control (HAC $p \approx 0.03$). Granger causality tests on detrended series do not provide decisive evidence of temporal directionality in the full sample (minimum lag-1–5 $p \approx 0.063$), and rolling-window tests show only isolated windows with $p < 0.05$. Breakpoint (Chow-type) scans indicate candidate changes in trend around 2008 in GMST and earlier dates for pole-speed proxies (1996/2006), suggesting time-varying relationships. Finally, quasi-decadal (8–13 year) bandpassed components show that a low-degree core proxy (PCA PC1 from internal IGRF coefficients $n \leq 3$) correlates with magnetic-pole speed ($r \approx 0.78$) and also with GMST ($r \approx 0.61$). A HAC regression on the bandpassed components finds significant contributions from both pole-speed and the core proxy, while their residual correlation after removing the core proxy drops to $r \approx 0.325$, suggesting partial mediation rather than a complete explanation. These results document a reproducible statistical "pulse" across geomagnetic and climate components of the Earth system, while leaving physical causal attribution to future work.

Keywords

Geomagnetism; magnetic pole drift; GMST; Newey–West HAC; breakpoint scan; Granger causality; IGRF; quasi-decadal variability.

1. Introduction

The global-mean surface temperature record contains both a strong long-term trend driven primarily by radiative forcing and substantial interannual to decadal variability. Separately, the geomagnetic field exhibits secular variation governed by fluid motions in the outer core. A long-standing question is whether measurable aspects of geomagnetic dynamics co-vary with components of climate variability, either through a shared internal driver or via indirect coupling pathways.

Here we perform a strictly empirical and fully reproducible analysis on annual data (1981–2024). Our goal is not to claim a new climate driver, but to quantify: (i) whether geomagnetic pole-speed proxies retain statistical association with GMST when standard controls are included; (ii) whether the association appears time-varying (rolling estimates, breakpoint scans); and (iii) whether quasi-decadal components align with a low-degree "core proxy" derived from IGRF internal coefficients.

2. Data and provenance

All inputs are publicly available and are documented with direct links (see Section 8). We provide a derived analysis-ready dataset in this package:

- `data/derived/PAPER_dataset_1981_2024_keyseries_coreproxy.csv` (series used for figures/tables in this preprint);
- `data/derived/MASTER_dataset_1981_2024_noAOD_with_core_proxy.csv` (wider set of intermediate fields and diagnostics).

CO_2 radiative forcing. We compute an annual CO_2 radiative forcing proxy as

$$RF_{CO_2}(t) = 5.35 \ln\left(\frac{C(t)}{C_0}\right),$$

with $C(t)$ the annual mean CO_2 concentration and $C_0 = 278$ ppm (preindustrial baseline), following Myhre et al. (1998).

3. Methods

3.1. Preprocessing

All series are aggregated to annual means, aligned on 1981–2024, and (where needed) standardized as $z = (x - \bar{x})/\sigma$. The pipeline is deterministic (fixed filter order, fixed lag settings) and controlled by the included scripts and `MANIFEST.json`.

3.2. HAC-robust multivariate regression

We fit OLS models of standardized GMST on standardized predictors and compute Newey–West HAC standard errors (maxlags=3). Two full specifications are used, differing only by the geomagnetic-activity control (aa vs ap):

$$z(\text{GMST}) = \alpha + \beta_1 z(\text{Speed}_{dip}) + \beta_2 z(\text{GeomAct}) + \beta_3 z(\text{Neutrons}) + \beta_4 z(\text{Niño3.4}) + \beta_5 z(RF_{CO_2}) + \varepsilon.$$

3.3. Rolling-window stability

We refit the HAC model on rolling 25-year windows and track β_1 (pole-speed) with its 95% confidence interval, to assess time variation.

3.4. Granger causality on detrended series

To reduce spurious regression risks under trending series, we linearly detrend GMST and pole-speed within the full sample (and, separately, within each rolling window) before applying standard Granger causality tests with lags 1–5 in both directions.

3.5. Trend-break scan

We scan for a single break in a linear trend model (intercept+slope) using a Chow-type F statistic, enforcing minimum segment lengths (10 and 15 years). This is a descriptive diagnostic, not a proof of regime change.

3.6. Quasi-decadal (8–13y) bandpass and core proxy

We extract quasi-decadal components using a Butterworth bandpass filter (order 4, 8–13 year passband) with zero-phase filtering (`filtfilt`). A "core proxy" is built by applying PCA (SVD) to the detrended+bandpassed internal IGRF coefficients with degree $n \leq 3$, and retaining PC1 (standardized). We then examine correlations and a HAC regression:

$$z(\text{GMST}_{8\text{–}13}) = \alpha + \gamma_1 z(\text{Speed}_{8\text{–}13}) + \gamma_2 z(\text{CorePC1}_{8\text{–}13}) + \eta.$$

4. Results

4.1. Overview and quasi-decadal components

Figure 1 shows the raw annual series (GMST and controls) and the geomagnetic pole-speed proxy. Figure 2 shows the 8–13y components and the core proxy PC1.

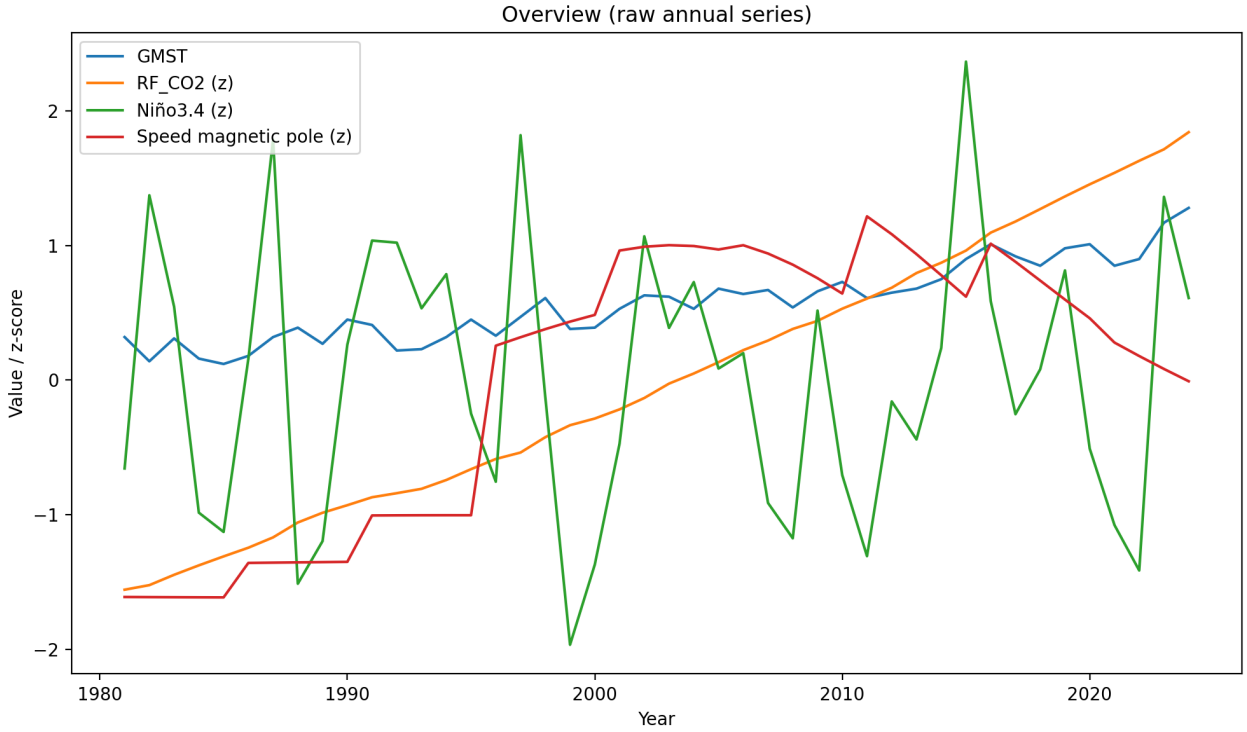

Figure 1: Overview of raw annual series. GMST is shown alongside standardized controls and standardized magnetic-pole speed.

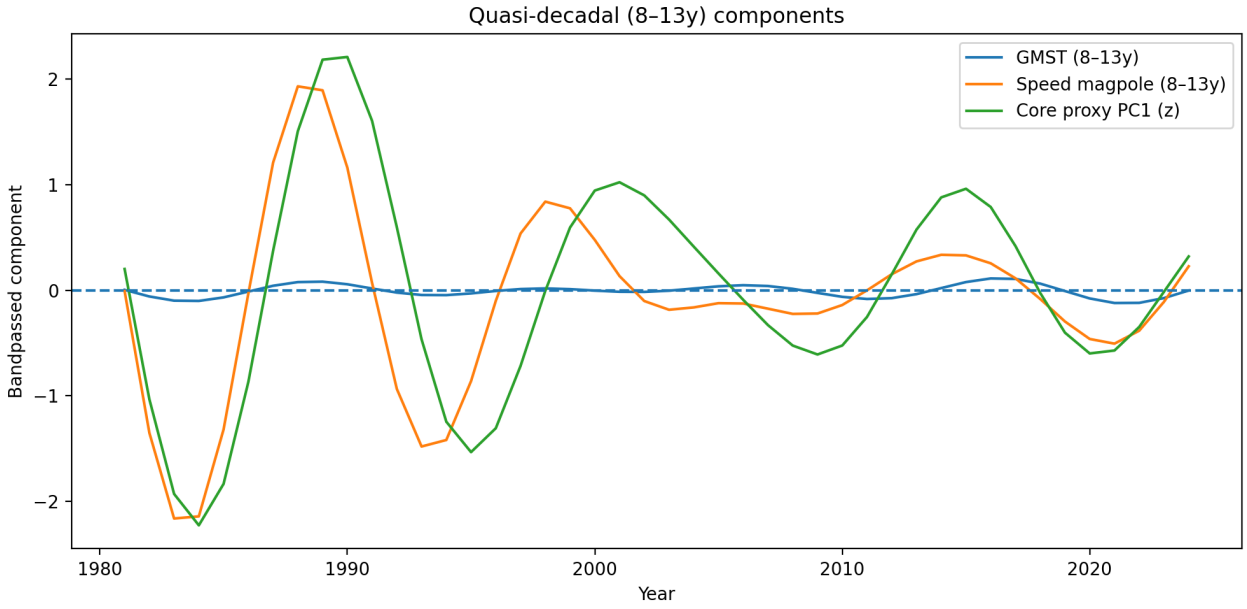

Figure 2: Quasi-decadal (8–13y) bandpassed components for GMST and pole-speed, with the standardized core proxy PC1.

Table 1: Compact summary of headline results from the reproducibility pipeline.

Test / quantity	Value	p	Notes
HAC full (with aa) beta(speed_dipole)	-0.175	0.0305	Standardized; GMST speed + aa + neutrons + nino34 + rf_co2; HAC maxlags=3
HAC full (with ap) beta(speed_dipole)	-0.174	0.0277	Standardized; GMST speed + ap + neutrons + nino34 + rf_co2; HAC maxlags=3
Rolling 25y HAC (with aa) share p<0.05	0.400		Fraction of rolling windows with significant beta(speed)
Rolling 25y HAC (with ap) share p<0.05	0.400		Fraction of rolling windows with significant beta(speed)
Granger full (detrended) min p speed→GMST	0.063	0.0634	Min over lags 1–5 (ssr_ftest)
Rolling 25y Granger speed→GMST count pmin<0.05	1.000		Count of rolling windows with pmin<0.05
Breakpoint Chow best (minseg=15) for gmst	2008.000		F=5.046
Breakpoint Chow best (minseg=15) for speed_magpole	1996.000		F=93.618
Breakpoint Chow best (minseg=15) for speed_dipole	2006.000		F=48.959
Core hypothesis corr(core_pc1, speed_magpole_bp8_13)	0.777		Pearson correlation on 8–13y components
Core hypothesis corr(core_pc1, gmst_bp8_13)	0.612		Pearson correlation on 8–13y components
Core HAC bandpass beta(speed_bp)	0.408	<1e-4	GMST_bp speed_bp + core_pc1; HAC maxlags=3
Core HAC bandpass beta(core_pc1)	0.295	0.0228	GMST_bp speed_bp + core_pc1; HAC maxlags=3
Residual corr after removing core proxy (bandpass)	0.325		corr(resid GMST_bp, resid speed_bp)

4.2. HAC multivariate models

Table 1 gives headline quantities, and Tables 2–3 report coefficients. In both full specifications, the pole-speed(dipole) coefficient is negative and statistically significant at $\approx 3\%$ (HAC). CO_2 forcing and Niño3.4 are strongly significant, while neutrons and geomagnetic activity (aa/ap) are weaker in this specification.

4.3. Rolling stability and Granger tests

Rolling-window estimates (Figures 3–4) show time variation in β(speed); 40% of 25-year windows yield a significant pole-speed coefficient at $p < 0.05$ (pipeline summary). Rolling-window Granger tests (Figure 5) show only one window with $p_{min} < 0.05$ for speed→GMST across lags 1–5, while the full-sample detrended test remains above 0.05.

Table 2: HAC (Newey–West, maxlags=3) multivariate regression on standardized annual series (1981–2024, $n = 44$): GMST ~ pole-speed(dipole) + aa + neutrons + Niño3.4 + RF_{CO_2}.

Term	β	SE (HAC)	p	95% CI low	95% CI high
Intercept	-0.000	0.037	1.0000	-0.073	0.073
Pole-speed (dipole) z	-0.175	0.081	0.0305	-0.333	-0.016
aa index z	-0.137	0.099	0.1684	-0.331	0.058
Neutron counts (Oulu) z	-0.156	0.092	0.0893	-0.336	0.024
Niño 3.4 z	0.131	0.035	0.0002	0.062	0.200
CO_2 radiative forcing z	1.083	0.072	<1e-4	0.941	1.224

Table 3: Robustness check replacing aa with ap (HAC Newey–West, maxlags=3), same specification and sample (1981–2024, $n = 44$).

Term	β	SE (HAC)	p	95% CI low	95% CI high
Intercept	-0.000	0.037	1.0000	-0.072	0.072
Pole-speed (dipole) z	-0.174	0.079	0.0277	-0.329	-0.019
ap index z	-0.145	0.097	0.1353	-0.335	0.045
Neutron counts (Oulu) z	-0.161	0.093	0.0839	-0.343	0.022
Niño 3.4 z	0.132	0.035	0.0002	0.064	0.201
CO_2 radiative forcing z	1.074	0.074	<1e-4	0.928	1.219

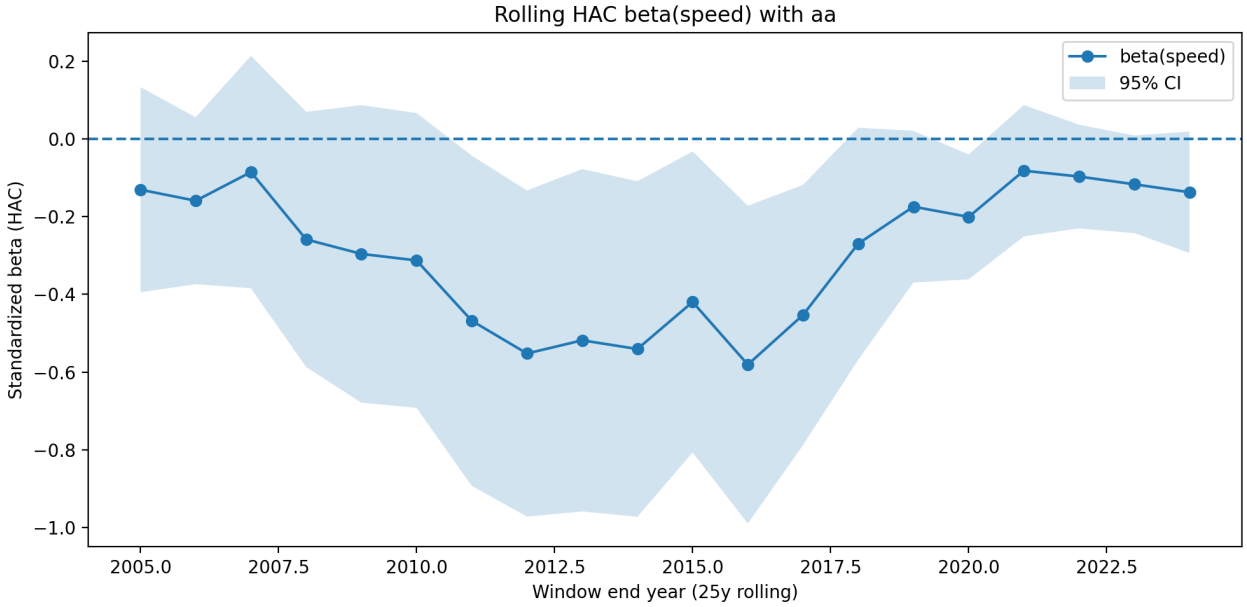

Figure 3: Rolling 25-year HAC estimate of β(speed) in the aa-controlled model (95% CI).

Table 4: Granger causality tests on linearly detrended annual series (full sample 1981–2024). Reported are ssr_ftest p-values.

Lag	p (speed→GMST)	p (GMST→speed)
1	0.0634	0.7594
2	0.1241	0.5446
3	0.0684	0.7510
4	0.0844	0.8438
5	0.0952	0.9089

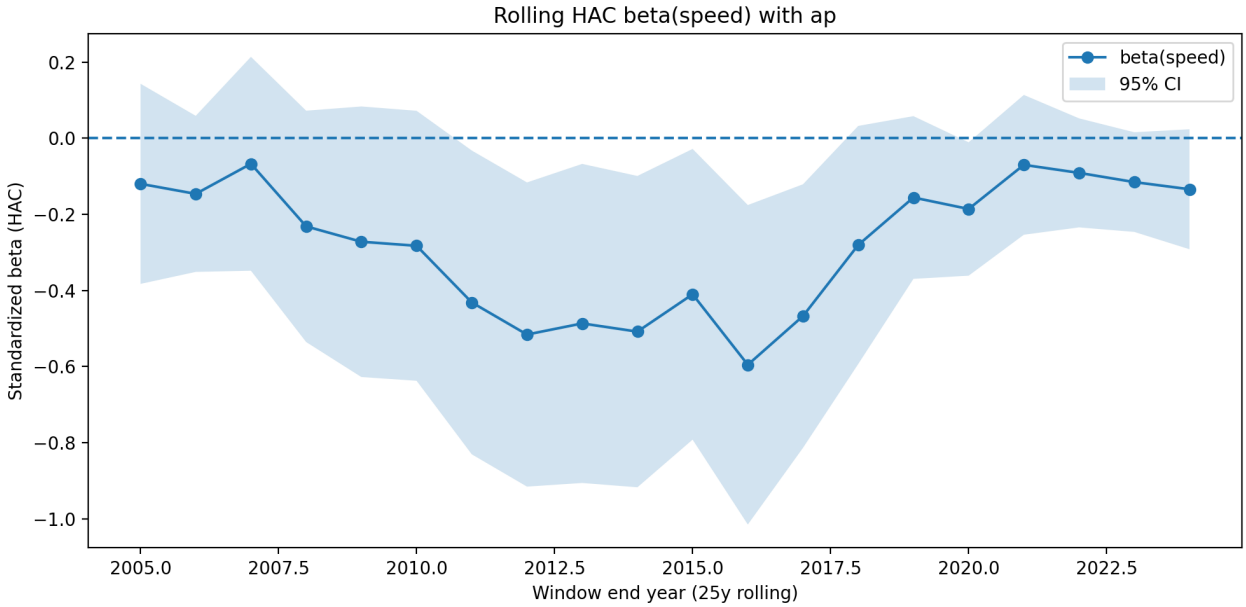

Figure 4: Rolling 25-year HAC estimate of β(speed) in the ap-controlled model (95% CI).

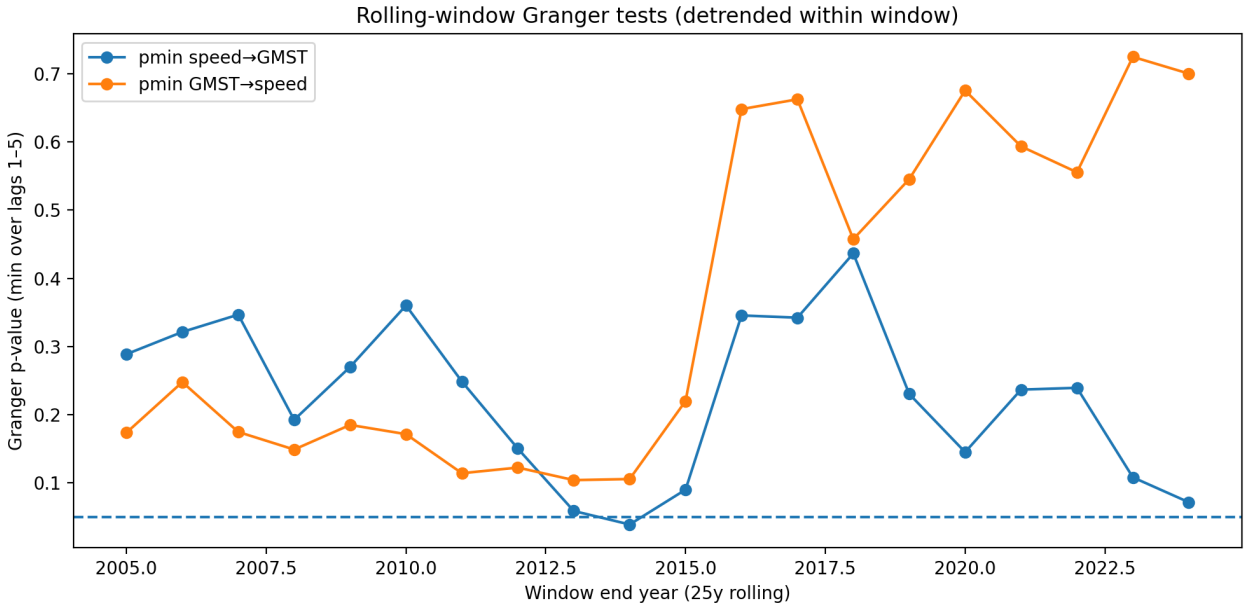

Figure 5: Rolling-window Granger tests on detrended series: minimum p-value over lags 1–5 for both directions.

Table 5: Single-break Chow-type scan for a break in the linear trend (intercept+slope). Best candidate year and corresponding F statistic.

Series	Min segment (y)	Best break year	Chow-like F
GMST	10	2014	5.223000
GMST	15	2008	5.046000
Pole-speed (dipole)	10	2006	48.959000
Pole-speed (dipole)	15	2006	48.959000
Pole-speed (magnetic pole)	10	1996	93.618000
Pole-speed (magnetic pole)	15	1996	93.618000

4.4. Breakpoint scans

Breakpoint scans (Table 5, Figures 6–7) identify distinct candidate years. GMST shows a strongest candidate break around 2008 (for min segment 15y), while pole-speed proxies indicate earlier candidate breaks (1996 for magnetic pole speed; 2006 for dipole speed). These scans suggest non-stationarity and motivate caution when interpreting single full-sample coefficients.

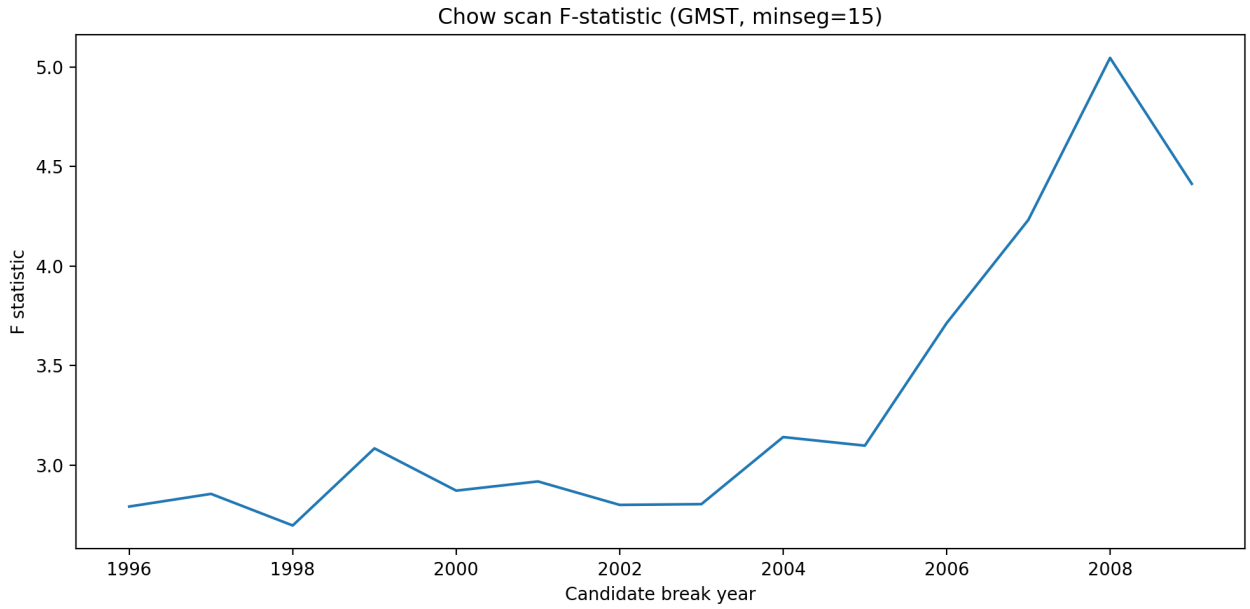

Figure 6: Chow-type break scan F statistic for GMST (min segment 15y).

Table 6: Pairwise correlations among quasi-decadal (8–13 year) bandpassed components (Pearson r).

Pair	Pearson r
Core proxy PC1 vs pole-speed (magpole), 8–13y	0.777
Core proxy PC1 vs GMST, 8–13y	0.612
GMST vs pole-speed (magpole), 8–13y	0.637

Table 7: HAC regression on quasi-decadal (8–13y) components: GMST_{8--13} ~ $\mathrm{pole\text{-}speed}_{8--13}$ + core proxy $\mathrm{PC1}_{8--13}$ (HAC maxlags=3).

Term	β	SE (HAC)	p	95% CI low	95% CI high
Intercept	0.000	0.179	1.0000	-0.350	0.350
Pole-speed (magpole, 8–13y) z	0.408	0.076	<1e-4	0.259	0.558
Core proxy PC1 (8–13y) z	0.295	0.129	0.0228	0.041	0.548

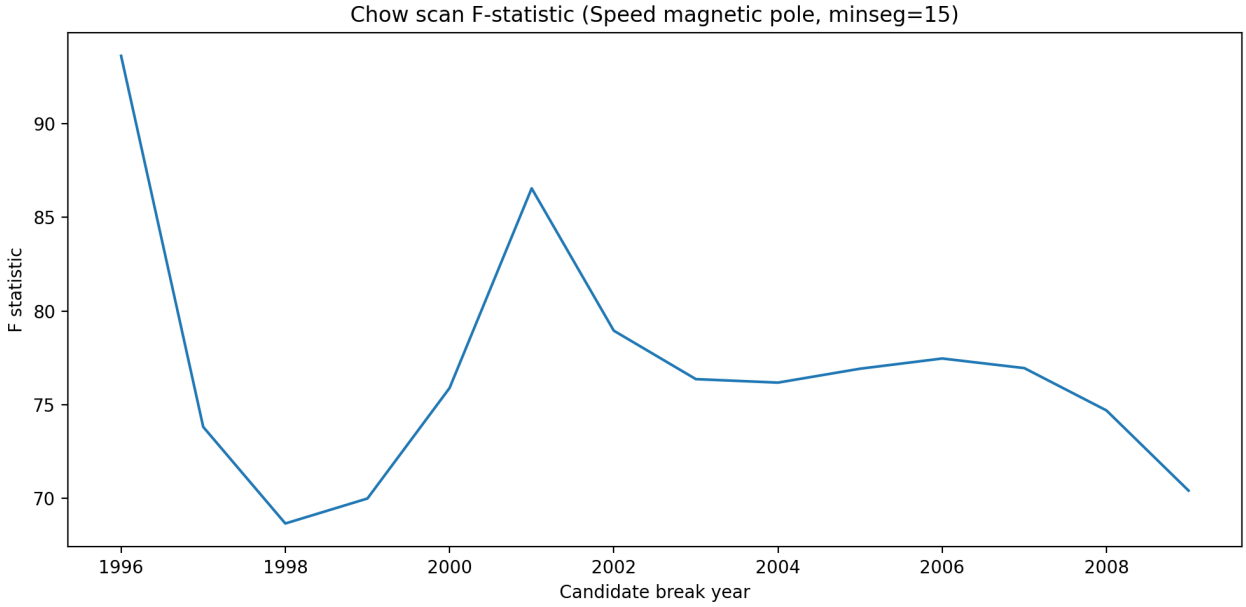

Figure 7: Chow-type break scan F statistic for magnetic pole speed (min segment 15y).

4.5. Core proxy hypothesis on quasi-decadal components

On 8–13y components, the core proxy PC1 correlates strongly with magnetic pole speed ($r \approx 0.78$) and moderately with GMST ($r \approx 0.61$) (Table 6). A HAC regression on bandpassed components yields significant contributions from both pole-speed and the core proxy (Table 7), while the residual correlation between $\mathrm{GMST}_{8–13}$ and $\mathrm{speed}_{8–13}$ after removing the core proxy drops to $r \approx 0.325$ (pipeline summary), consistent with partial mediation by the core proxy.

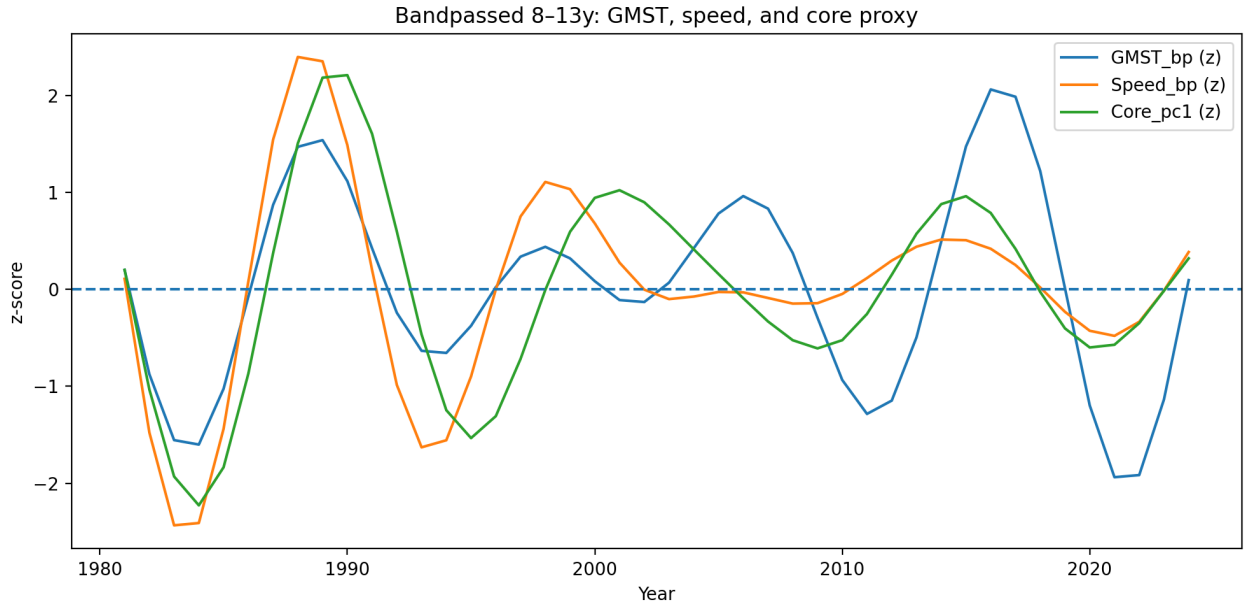

Figure 8: Bandpassed 8–13y standardized triplet: GMST, magnetic pole speed, and core proxy PC1.

5. Discussion

Across 44 years of annual data, the geomagnetic pole-speed proxy behaves like a quiet metronome that occasionally falls into step with GMST even after accounting for dominant controls. The multivariate HAC results document a reproducible statistical association between GMST and pole-speed(dipole); the negative standardized coefficient is stable to the choice of geomagnetic-activity control (aa vs ap). This is not a claim of a new forcing, but a quantitative description of what remains in the data once the usual suspects are included.

At the same time, the evidence for temporal directionality is deliberately modest: full-sample detrended Granger tests are marginal (min $p \approx 0.063$), rolling-window significance is isolated, and breakpoint scans suggest non-stationarity in both GMST and pole-speed proxies. Together, these diagnostics argue for caution and for time-aware modelling rather than a single timeless coefficient.

The quasi-decadal analysis sharpens the picture: on 8–13 year components, a low-degree internal-field proxy (IGRF $n \leq 3$ PC1) aligns strongly with magnetic pole-speed ($r \approx 0.78$) and also with GMST ($r \approx 0.61$). In a HAC regression on the bandpassed components, both pole-speed and the core proxy contribute significantly, while the residual GMST–speed correlation after removing the core proxy drops to $r \approx 0.325$. This pattern is consistent with (but does not prove) a shared internal-timescale signal that imprints itself on geomagnetic secular variation and on a quasi-decadal component of GMST. Pinning down the physical pathway, if any, remains the central open task.

6. Limitations

Key limitations include: short sample size ($n = 44$); multiple testing and model-selection degrees of freedom; potential sensitivity to filtering choices outside the fixed pipeline settings; and the fact that Granger causality is a predictive criterion that does not constitute physical causation. Results should be interpreted as a reproducible statistical finding that motivates further mechanistic work, not as a standalone proof of a new climate forcing.

7. Reproducibility, data and code availability

This preprint is intended to be deposited on Zenodo together with all code, derived data, and figures required to reproduce every table and plot.

- **Code.** See `scripts/`. A convenience runner is included as `GO_EUREKA.py`.
- **Derived datasets.** See `data/derived/`. The analysis uses `PAPER_dataset_1981_2024_keyseries_coreproxy.csv`
- **Outputs.** Figures in `outputs/figures/` and tables in `outputs/tables/`.
- **Integrity.** `MANIFEST.json` provides SHA-256 hashes (created `2026-02-18`) to validate that files are unchanged.

Minimal reproduction (Linux/macOS).

```
python -m venv .venv
source .venv/bin/activate
pip install -r requirements.txt
python scripts/build_derived_from_raw.py
python scripts/run_preprint_pipeline.py
```

8. Data sources

The table below lists the external sources used to assemble the raw inputs (all publicly available) and the specific "as-of" timestamps used in this release. The derived CSVs that reproduce the results and figures are included in the Zenodo archive under `data/derived/` and `outputs/tables/`.

Key derived CSV outputs included in this archive.

- `outputs/Results_Summary.csv` (headline statistics for models, Granger, break scans, and bandpass tests)
- `outputs/tables/hac_model_with_aa_coeffs.csv` and `...ap...` (full-model coefficients)
- `outputs/tables/granger_full_detrended_pvalues.csv` and `granger_rolling_25y_pmin.csv`
- `outputs/tables/breakpoints_chow_scan.csv`
- `outputs/tables/core_hypothesis_bandpass_correlations.csv`

Table 8: Primary data sources used to build the derived CSVs (links verified in the provided sources document).

Series	Source	Direct link
GMST	NASA GISTEMP v4	https://data.giss.nasa.gov/gistemp/tabledata_v4/GLB.Ts%2BdSST.csv
CO_2 (annual mean)	NOAA GML Trends	https://gml.noaa.gov/webdata/ccgg/trends/co2/co2_annmean_gl.csv
Niño 3.4	NOAA PSL / CPC	https://psl.noaa.gov/data/timeseries/month/Nino34_CPC/
Cosmic-ray neutrons	Oulu Neutron Monitor	https://cosmicrays.oulu.fi/
aa index	ISGI (aa index download)	https://isgi.unistra.fr/data_download.php
ap/Ap indices	GFZ Potsdam (Kp/ap/Ap)	https://kp.gfz.de/app/files/Kp_ap_Ap_SN_F107_since_1932.txt
IGRF-13 coefficients (internal field)	NOAA NCEI / IAGA vmod	https://www.ngdc.noaa.gov/IAGA/vmod/coeffs/
Radiative forcing formula reference	Myhre et al. (1998) DOI	https://agupubs.onlinelibrary.wiley.com/doi/10.1029/98GL01908

References

1. Newey, W.K., West, K.D. (1987). A simple, positive semi-definite, heteroskedasticity and autocorrelation consistent covariance matrix. *Econometrica*.
2. Granger, C.W.J. (1969). Investigating causal relations by econometric models and cross-spectral methods. *Econometrica*.
3. Chow, G.C. (1960). Tests of equality between sets of coefficients in two linear regressions. *Econometrica*.
4. Lenssen, N.J.L., et al. (2019). Improvements in the uncertainty model in the NASA GISTEMP surface temperature analysis. *J. Geophys. Res. Atmos.* https://doi.org/10.1029/2018JD029522
5. Alken, P., et al. (2021). International Geomagnetic Reference Field: the thirteenth generation. *Earth, Planets and Space*. https://doi.org/10.1186/s40623-020-01288-x
6. Myhre, G., Highwood, E.J., Shine, K.P., Stordal, F. (1998). New estimates of radiative forcing due to well mixed greenhouse gases. *Geophys. Res. Lett.* https://doi.org/10.1029/98GL01908
7. Mayaud, P.-N., Menvielle, M., Chambodut, A. (2023). aa geomagnetic index (Dataset). ISGI. https://isgi.unistra.fr/data_download.php
8. Matzka, J., et al. (2021). Geomagnetic Kp index and derived indices of geomagnetic activity (Kp, ap, Ap) (Dataset). GFZ Data Services. https://doi.org/10.5880/Kp.0001
9. Oulu Neutron Monitor. Cosmic ray data service. https://cosmicrays.oulu.fi/
10. NOAA PSL/CPC Niño 3.4 index time series. https://psl.noaa.gov/data/timeseries/month/Nino34_CPC/
11. NOAA GML CO_2 trends, annual mean (global). https://gml.noaa.gov/webdata/ccgg/trends/co2/co2_annmean_gl.csv